11

Graphene nanostrips based IR range detector

© I.V. Ivashentseva,[1] P.V. Fedotov,[2,3] N.S. Kaurova,[1] M.G. Rybin,[2] E.D. Obraztsova,[2,3]
I.V. Tretyakov,[4] G.N. Goltsman[1]

[1]Moscow Pedagogical State University,
119435 Moscow, Russia
[2]„Prokhorov Institute of General Physics“,
Russian Academy of Sciences 119991 Moscow, Russia
[3]Moscow Institute of Physics and Technology (National Research University),
141701 Dolgoprudny, Moscow Region, Russia
[4]Lebedev Physical Institute, Russian Academy of Sciences,
117997 Moscow, Russia
email: ivantretykov@mail.ru

Received February 7, 2024
Revised May 6, 2024
Accepted May 14, 2024

The work presents a technology for sensitizing a structure consisting of a graphene nanostrip on a Si/GNR silicon substrate in the near-IR range of the electromagnetic spectrum based on doping a GNR graphene nanostrip with He^4. The response has been experimentally demonstrated to increase by more than 25 times at a wavelength of 1.35 μm in the Si/GNR/He^4 structure compared to undoped Si/GNR. Also, the Si/GNR_He^4 structure exhibits pronounced multi-level memristor properties under the influence of IR radiation.

Keywords: graphene, graphene nanostrip, IR range, detector.

DOI: 10.61011/TP.2024.08.59018.31-24

Introduction

Silicon (Si) is the most commonly used technological semiconductor material, and is the base of modern integrated microelectronics, and the use of planar photonic Si waveguides opens up completely new opportunities in the field of modern integrated optics. The high refractive index of silicon makes it possible to manufacture small optical components, whose typical dimensions are an order of magnitude smaller in comparison with their fiber-optic counterparts; moreover, it is possible to achieve an incomparably high optical radiation density in the section of Si waveguides. The silicon photonics provides the possibility for a tight integration of a large number of optical elements making up the optical circuit of the end device on one relatively small chip. Si has a band gap of $\Delta E = 1.12$ eV, for this reason it is transparent to infrared (IR) radiation starting from the wavelength of $\lambda = 1.1\,\mu$m, in addition, its ε does not change over a wide range of IR radiation powers. These properties make it possible to manufacture dielectric single-mode waveguides and passive elements with low losses, however, they do not make it possible to easily create active optical elements of the IR range from Si, such as radiation detectors, optical memory elements, modulators, gas sensors, etc. This requires either local Si doping or integration of non-silicon electro-optical materials.

For instance, modern approaches for creation of IR radiation detectors involve high-temperature doping of Si with S, Se, Te [1–4] atoms and some transition metals (Au, Ag, Ti, etc.) [5–12]. A striking example is the high-temperature doping of Si with Ag silver particles, while it is possible to improve the sensitivity of the photodetector by 2.5 times compared with pure Si [13]. However, the ion implantation method is associated with high temperatures, which is often a fundamental limitation in modern integrated optics circuits.

The use of two-dimensional materials is extremely promising for the creation of active elements of integrated optical circuits, since 2D materials can be easily transferred to any substrate. Graphene (Gr) and related 2D materials vividly demonstrate their advantages for a broad range of optoelectronic applications [14], such as data transmission [15–17], high-performance LEDs [18], ultrafast optical modulation [19] and photodetection with speeds of up to 80 GHz [20] and ultra-wideband photodetection [21–28]. Also, several high-performance electronic devices and sensors were demonstrated based on two-dimensional materials, such as hypersensitive Hall sensors [29,30], strain sensors [31], biosensors [32], gas sensors [33] and high-frequency transistors [34,35].

Graphene/PbS quantum dots (QD) are successfully used in CMOS matrices as an alternative to Si photodetectors [36]. The use of QD of various compositions in combination with Gr allows fine-tuning the spectral range of the detector depending on the absorption region of QD [37–41]. The process of production of high-quality QDs is based on molecular beam epitaxy methods and involves high production costs. The production of colloidal QDs, such as Ag2S, PbS, etc., is a cheaper method, however, the resulting purity of the colloidal solution and the quality

of QD are significantly lower, which significantly constrains their use. In addition, the QD flicker problem has not been completely solved. Graphene nanoribbons (GNRs) attract interest due to their pronounced dependence of electronic and optical properties on the GNR structure, especially on the type of edge and width of the ribbon [42]. There is no band gap in the electronic structure of graphene. But despite this, there is a band gap in narrow graphene nanoribbons (GNRs) with a certain type of edge. The band gap increases with a decrease of nanoribbon width [43]. GNRs have many applications, especially as a field effect transistor [44–46]. Theoretical studies discovered a strong electron-hole interaction in graphene nanoribbons [47,48]. The structural parameters of a certain type of GNR (edge type and ribbon width) determine the spectral position of the singularities in the spectra. Graphene nanoribbons AGNR with armchair-type edges (phenanthrene edges) are characterized by the number N of lines of carbon dimers located along the width of the nanoribbon. They are divided into three different groups, for each of which the number N can be represented as $3p$, $3p+1$ or $3p+2$ (p — a natural number). For example, graphene nanoribbons 7-AGNR belong to the group $3p+1$, for which the band gap widths of the GNR are the largest among these three groups.

We studied in this paper the spectral response of a silicon Si structure coated with GNR in an atmosphere of He^4 at tenths of a ppm unit. He^4 was used to dope GNR instead of quantum dots. The use of gases allows precise control of the required doping level. If necessary, Si/GNR were completely purified by He^4, for this purpose the structure was heated to $120-150^\circ$C and was kept in a vacuum.

1. Graphene nanoribbon production technology

Graphene nanoribbon films 7-AGNR were synthesized from 10.10ˊdibromo-9.9ˊbianthracene (DBBA) molecules on nickel (Ni) foil by the modified chemical vapour deposition (CVD), based on the nanotechnology of „bottom−up“ type [49]. This method has already been previously used for the production of films of 7-AGNR [49,50] and 3-AGNR [51]. As a preparation, the Ni foil was first annealed at a temperature of 1000,°C by a flow of 100,sccm of hydrogen (H_2) for 15 min, and then it was cooled in the medium vacuum. The Ni-foil was then placed in a glass tube with DBBA powder (≈ 1 mg). Next, the glass tube together with the Ni-foil was sealed during pumping by a vacuum pump (10−3 mbar). The hermetically sealed glass tube was placed in a quartz tube reactor and annealed in a two-step process. The first stage involves the dehalogenation and polymerization of DBBA molecules. This occurs during the annealing of the samples at a temperature of 190 °C for 12−24 h. Films from polyantrylene (PA) oligomers can be obtained at this stage of synthesis. The second stage consists of intramolecular cyclodehydrogenation of PA during annealing at a temperature of 340 °C for 1−3 h. This stage of synthesis transforms PA oligomers into 7-AGNR. It is possible to obtain thin films from graphene nanoribbons on nickel foil after these two stages of synthesis.

As a rule, synthesized films consist of graphene nanoribbons GNR, and polyantrylene oligomers are only an intermediate result. The GNR films were thoroughly washed in isopropanol after the synthesis process. This step is necessary for cleaning the nanoribbon films from the remnants of PA oligomers that may still be present in them. A film of graphene nanoribbons synthesized on nickel foil was placed in toluene and gently mixed for 10 min for obtaining an optical quality suspension. Part of the nanoribbons passed into a toluene solution at the same time. The remaining part of the nanoribbon film on the foil was removed from the solution after that. Further, the suspension of graphene nanoribbons in toluene was subjected to ultrasonic treatment for 10 min at low ultrasound power for a better individualization of nanoribbons. The characteristic film size of graphene nanoribbons on nickel foil is 1 cm^2. The width of graphene nanoribbons 7-AGNR is approximately 0.75 nm [43]. Graphene nanoribbons (GNR) were deposited from suspension onto a silicon Si substrate by a drop method.

2. Raman spectroscopy of GNR nanoribbons

Raman spectra and photoluminescence spectra were obtained using a LabRam HR Evolution spectrometer provided with a single monochromator and a set of filters for measuring ultra-low frequencies. A confocal optical scheme was used to optimize measurements. A diode laser (532 nm) was used for optical excitation. The spectral resolution was of the order of 1.0 cm^{-1} in the RS spectra. The spectral resolution was 0.5nm in the photoluminescence spectra.

Synthesized and washed in toluene films from graphene nanoribbons have unique characteristic RS markers, which are characteristic of 7-AGNR, according to various experimental and theoretical studies (Fig. 1) [52–55].

The band with the highest intensity in the RS spectra is the G-mode of 7-AGNR films, at a frequency of 1606 cm^{-1}. The G-mode is typical for sp^2-carbon materials, including graphene and carbon nanotubes. The G-mode of graphene and the GNR graphene nanoribbon are similar, but usually the G-mode of the graphene nanoribbon is divided into two components: G^+ and G^- modes. G^+ component of G^- mode is observed in „armchair“ type GNR based on theoretical studies, which is the optical main mode transverse in the plane of the graphene nanoribbon [56]. The mode G^+ has a higher RS frequency. An intense G^+ mode is observed in 7-AGNR films in experimental study, and the intensity of the mode G^- is usually quite low.

The second most intense feature in the spectra of 7-AGNR films is the so-called D-mode with a frequency of 1343 cm^{-1}. The D-mode is often found in graphene and carbon nanotubes, for which this RS mode is an interline

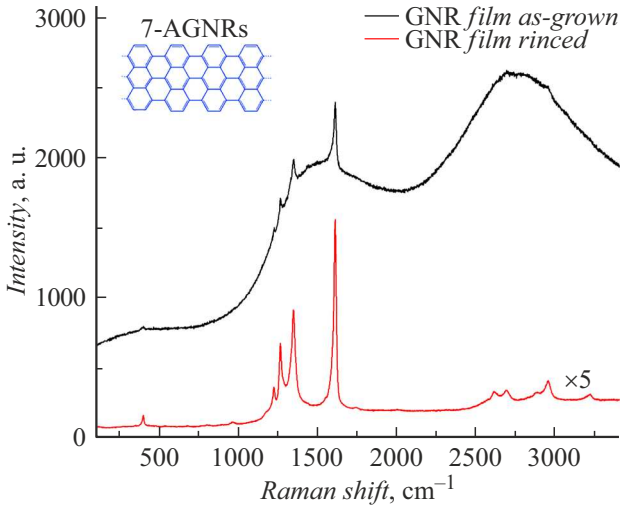

Figure 1. Typical RS spectra of synthesized (black spectrum) and toluene washed (red spectrum) films 7-AGNR. The spectra were obtained at an excitation of 532 nm. The intensity of the RS spectrum of 7-AGNR films washed with toluene was increased by 5 times for clarity. The insert shows a diagram of graphene nanoribbons of the type 7-AGNR.

process with double resonance. It is activated by defects in the material, as a rule. The high intensity of the D-mode is a sign of a high concentration of defects for graphene and carbon nanotubes. At the same time, the intensity of the D-mode in the RS spectra of graphene nanoribbons of the GNR type can be high, regardless of the concentration of defects [52–55]. The high intensity of the D-mode is typical for atomically precise graphene nanoribbons [52–54].

One of the most characteristic RS modes of narrow graphene nanoribbons is the radial breathing-like mode (RBLM), which has different resonant frequencies, depending on the width of the ribbon. The RBLM resonant frequency increases with the decrease of GNR width. In the case of synthesized GNR films, the resonant frequency of the radial respiratory-like mode was determined at a frequency of 397 cm^{-1}, which corresponds well to the expected frequency of the RBLM mode of 7-AGNR.

Two modes have also been recorded in the RS spectrum of 7-AGNR films, which are located at frequencies 1220 and 1260 cm^{-1}, which are associated with C-H chemical bonds of at the edges of graphene nanoribbons. These spectral modes are associated with specific bending vibrations of the C-H bonds in the plane of the nanoribbons. Other typical RS modes of 7-AGNR can also be observed: a set of second-order modes in the spectral frequency range 2580–3250 cm^{-1}, which are associated with combinations of modes observed at lower resonant frequencies [54].

Background photoluminescence (PL) is observed on the RS spectra of synthesized graphene nanoribbon films (Fig. 1). The PL intensity of nanoribbon films decreases significantly after partial removal of GNR into suspension by washing in toluene or ultrasonic treatment of films in toluene. When excited with a wavelength of 532 nm, the resulting suspension from 7-AGNR in toluene shows a bright PL in the range of 560–660 nm (Fig. 2). The PL intensity of graphene nanoribbons in the range of 540–720 nm significantly decreases after deposition of 7-AGNR onto a Si silicon substrate by the drop method. The PL peak of 7-AGNR deposited on a silicon substrate is noticeably wider, and a slight red shift of the PL band is observed. The high intensity of 7-AGNR PL in suspension is associated with the individualization of nanoribbons in toluene solution (Fig. 2). A decrease of the intensity of deposited GNRs is associated with the aggregation of nanoribbons as a result of deposition and interaction with the silicon substrate.

3. Structure and measurement technique of a detector based on GNR nanoribbons of graphene

Si structures were manufactured using standard methods of laser lithography, thermal deposition of metals and a lift-off process based on high-resistance Si, the thickness of the substrate was 350,μm. The contacts of the Si structure were formed by successive thermal deposition of Ti and Au. The width of the Ti/Au contacts W and the distance between them L were set using laser lithography, thereby determining the geometric dimensions of the initial Si structure. W and L were chosen to be 10 μm in this study. Figure 3 shows the optical image and the design of the studied samples. When creating the Si/GNR structure, it is important to prepare the Si surface of the sample between the Ti/Au contacts. The surface of the Si plate was prepared sequentially by ion

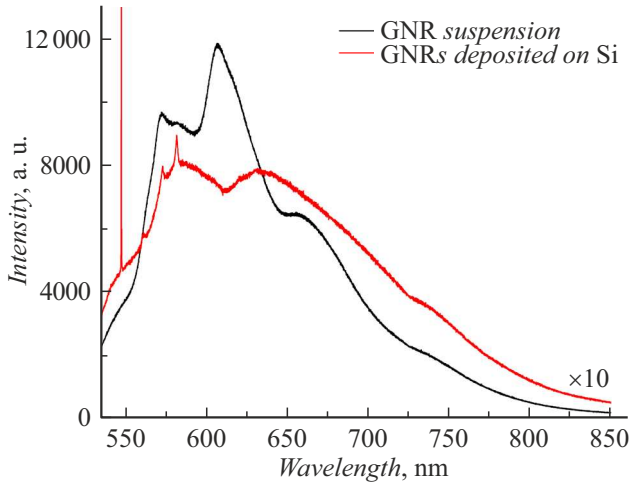

Figure 2. Typical PL spectra are suspensions of graphene nanoribbons7-AGNR (black spectrum) and graphene nanoribbons 7-AGNR deposited on a silicon substrate (red spectrum). The spectra were obtained at an excitation of 532 nm. The PL intensity of nanoribbons of 7-AGNR deposited on a silicon substrate was increased by 10 times for clarity. A spectrally narrow feature at a wavelength of 547 nm is associated with a silicon substrate.

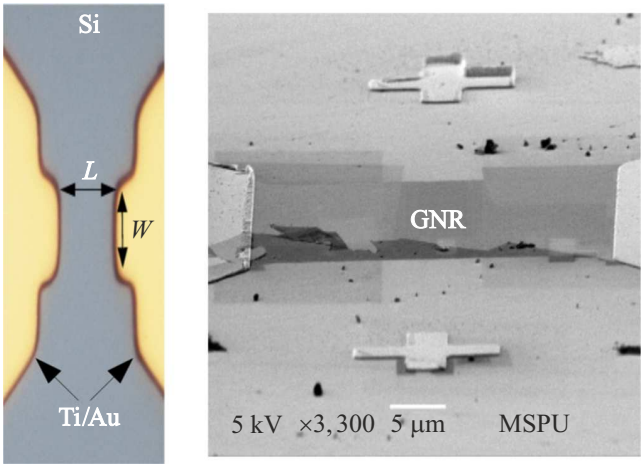

Figure 3. Image of Ti/Au contacts on the surface of a high-resistance Si substrate obtained using an optical microscope before applying Gr nanoribbons (left), L — contact spacing, W — contact width ($L = W = 10\,\mu$m); SEM is an image of the deposited cluster of Gr nanoribbons between the Ti/Au contacts of the structure (on the right). Radiation was collected using an elliptical lens on the Si surface between Ti/Au contacts.

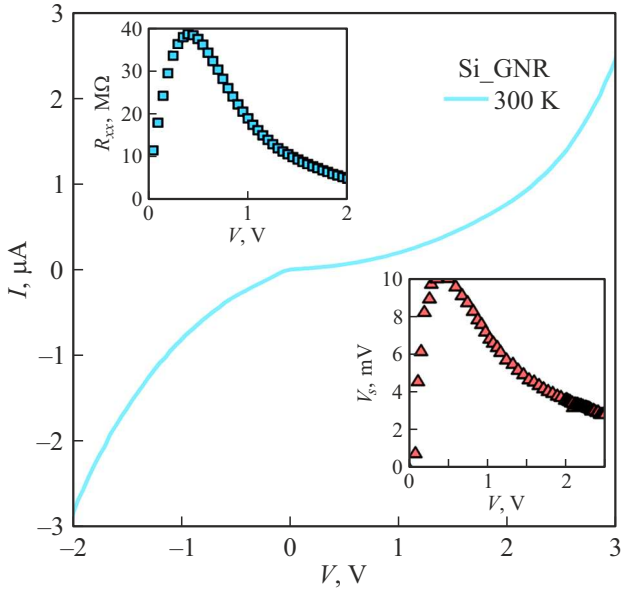

Figure 4. Current-voltage curve of the Si/GNR structure obtained in vacuum.

etching in an atmosphere of Ar and O_2 and liquid etching in hydrofluoric acid. The sequence of cleaning processes allows removing the contamination and natural oxide on the Si surface.

Figure 3 (on the left) shows an image of the Si surface between Ti/Au contacts obtained using an optical microscope before applying Gr nanoribbons (GNR), on the right is a SEM image with a cluster of Gr nanoribbons. As can be seen, the cluster of Gr nanoribbons which is a darker structure located on the surface of Si does not interact with other nanoribbons.

A hyper-hemispherical silicon lens was used to directly match the studied samples with IR radiation. The radiation incident on the lens was collected into an Airy spot on the surface of the Si pad between the Ti/Au contacts. The samples were shielded from background radiation by an optical window made of high-resistance Si with a thickness of 500 μm, in the absence of IR radiation, the resistance of the samples R was about 20 MΩ. Figure 4 shows the characteristic current-voltage curve of the studied Si/GNR structures in vacuum of $1 \cdot 10^{-6}$ mBar.

The amplitude of the sample response as a function of the wavelength of the IR radiation Sv(λ) was studied on an IR spectrometer in the range of $1 - 2\,\mu$m. The sample was at room temperature of 300 K during the measurement process in an optical vacuum volume, displaced by direct current. The doping process was carried out by the admission of He^4 into a vacuum volume, He^4 interacted with DC-biased Si/GNR for 10 min, after which the vacuum volume was pumped out again to a pressure of $1{\cdot}10^{-6}$ mBar.

The doping of graphene nanoribbons can result in the rearrangement of the electronic levels of nanoribbons and results in to the appearance of optical activity 7-AGNR in the IR region of the spectrum [50]. Trions can appear in doped 7-AGNR, which are observed in the PL spectra in the IR region of the spectrum [50].

4. Results of the response amplitude study

Figure 5 shows the results of an experimental study of Sv(λ) for Si/GNR and Si/GNR/He^4. Sv(λ) dependence of

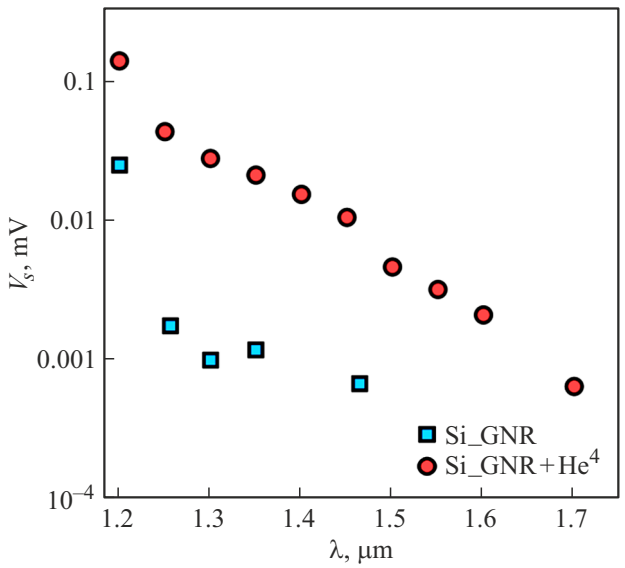

Figure 5. Spectral response of Si/GNR heterostructures at zero offset. The square symbols correspond to the spectral response of the pure Si/GNR structure annealed in vacuum. The round symbols represent the spectral response of the doped He^4 Si/GNR structure.

a Si/GNR structure is given to evaluate the effect of the absorption band expansion in case of He^4doping of the Si/GNR heterostructure.

Fig. 5 shows that $Sv(\lambda)$ dependence for the Si/GNR structure having a maximum of $\lambda = 1.1\,\mu$m, sharply drops already at $\lambda = 1.25\,\mu$m, the same data were obtained for Si-a sample not covered with graphene nanoribbons. After doping of Si/GNR graphene nanoribbons $Sv(\lambda)$ demonstrates a monotonous character of the drop up to $\lambda = 2\,\mu$m. The greater response for Si/GNR_He^4 compared to the Si/GNR structure at wavelengths greater than $1.1\,\mu$m can be explained by modification of the GNR energy spectrum in the interaction with He^4. To quantify the doping effect, it is convenient to reduce the ratio of the signal for Si/GNR_He^4 structure to the signal for Si/GNR structure taken at a given λ. This ratio was more than 25 times at $\lambda = 1.3\,\mu$m in our experiment. It is safe to say that GNR_He^4 on the surface of Si made a determining contribution to the detection of IR radiation at wavelengths above $\lambda = 1.1\,\mu$m in the complementary structure of Si/GNR_He^4, the doping level determines the photoconductivity of GNR.

For instance, GNR is locally heated when IR photons are absorbed, given the low thermal conductivity of Gr, it can be assumed that its temperature locally rises so high that this results in the departure of He^4 from GNR. This behavior was observed when studying the dependence of the response of Si/GNR_He^4 as a function of the acting IR power, V/W. V/W-the sensitivity of the heterostructures studied in this work in units of V/W was measured separately at a wavelength of $1.55\,\mu$m. A thermally stabilized laser diode was used as an IR radiation source. When measuring the V/W sensitivity, the radiation power of the laser diode was selected so that the signal-to-noise ratio V_s/V_n did not exceed 1.5-2 times, this was to guarantee the linear operation of the studied structures. The values of the signal V_s and noise V_n of the structure were measured at the laser diode radiation modulation frequency f from 5 to 100Hz. When the modulation frequency was increased to 60 Hz, the response amplitude already dropped by half. The experimentally obtained values of the noise equivalent power (NEP) for Si/GNR_He^4-heterostructures were $2.5 \cdot 10^{-9}\,\mathrm{W}/\sqrt{\mathrm{Hz}}$. In addition, there was a pronounced effect of „state memory“, i.e. when the laser diode was turned off, Si/GNR_He^4 resistance did not return to the initial value. Si/GNR_He^4 residual resistance depended on the IR radiation power applied to it. Si/GNR_He^4-heterostructure demonstrates pronounced multilevel memristor properties. The state maintaining time exceeded 1.5-2 min, depending on the initial doping level.

Conclusion

This paper demonstrated the technology of Si/GNR sensitization in the near-IR range of the electromagnetic spectrum, based on the doping of GNR using He^4. An over 25-fold increase of the response at a wavelength of $1.35\,\mu$m in the Si/GNR/He^4 structure was shown, compared with Si/GNR not doped with He^4. Si/GNR_He^4-structure demonstrates pronounced multilevel memristor properties under the action of IR radiation. Further development of the work may follow the path of a detailed study of the absorption spectra of Si/GNR/He^4 in the IR range, as well as studies of other doping materials.

Funding

These studies, namely the formulation of the problem, discussion of the results and synthesis of graphene nanoribbons, were carried out as part of the work under a grant and with the support of the Russian Science Foundation grant No.21-72-10164, https://rscf.ru/project/21-72-10164 /. Fabrication of the metal Ti/Au contacts using photolithography, thermal evaporation and the Lift-off process was carried out as part of a project of the university participation in the development of high-tech production with the support of the Ministry of Science and Higher Education of the Russian Federation (Agreement dated 06.04.2022 No 075-11-2022-026). The study of manufactured Si/GRN samples by electron microscopy and measurement of their spectral response was supported by the Russian Science Foundation grant № 23-12-00187, https://www.rscf.ru/project/23-12-00187/. The studies of graphene nanoribbons by Raman light scattering of light were supported by the Russian Science Foundation grant № 24-42-10001, https://rscf.ru/project/24-42-10001/.

Conflict of interest

The authors declare that they have no conflict of interest.

References

[1] L. Du, Z. Wu, R. Li, F. Tang, Y. Jiang. Opt. Lett., **41** (I), 5031(2016). DOI: 10.1364/OL.41.005031
[2] H. Zhang, J.-H. Choi, Y. Xu, X. Wang, X. Zhai, B. Wang, C. Zeng, J.-H. Cho, Z. Zhang, J. G. Hou. Phys. Rev. Lett., **106** (2−14), 026801 (2011). DOI: 10.1103/PhysRevLett.106.026801
[3] X.Y. Wang, Y.G. Huang, D.W. Liu, X.N. Zhu, H.L. Zhu. Chin. Phys. Lett., **30** (3), 036101 (2013). DOI: 10.1088/0256-307X/30/3/036101
[4] S. Hu, P. Han, S. Wang, X. Mao, X. Li, L. Gao. Semicond. Sci. Technol., **27**, 102002 (2012). DOI: 10.1088/0268-1242/27/10/102002
[5] J.P. Mailoa, A.J. Akey, C.B. Simmons, D. Hutchinson, J. Mathews, J.T. Sullivan, D. Recht, M.T. Winkler, J.S. Williams, J.M. Warrender, P.D. Persans, M.J. Aziz, T. Buonassisi. Nat. Commun., **5**, 3011 (2013). DOI: 10.1038/ncomms4011
[6] E. Garcia-Hemme, R. Garcia-Hernansanz, J. Olea, D. Pastor, A. del Prado, I. Martil, G. Gonzalez-Diaz. J. Phys. D: Appl. Phys., 104, 211105 (2014). DOI: 10.1088/0022-3727/49/27/2751
[7] C.B. Simmons, A.J. Akey, J.P. Mailoa, D. Recht, M.J. Aziz, T. Buonassisi. Adv. Functional Mater., **24**, 2852 (2014). DOI: 10.1002/adfm.201303820

[8] E. Pérez, H. Castán, H. Garcıa, S. Dueñas, L. Bailón, D. Montero, R. Garcıa-Hernansanz, E. Garcıa-Hemme, J. Olea, G. González-Dıaz. Appl. Phys. Lett., **106**, 022105. DOI: 10.1063/1.490578
[9] C.B. Simmons, A.J. Akey, J.J. Krich, J.T. Sullivan, D. Recht, M.J. Aziz, T. Buonassisi. J. Appl. Phys., **114**, 243514 (2013). DOI: 10.1063/1.4854835
[10] A.J. Said, D. Recht, J.T. Sullivan, J.M. Warrender, T. Buonassisi, P.D. Persans, M.J. Aziz. Appl. Phys. Lett., **99**, 073503 (2011). DOI: 10.1063/1.3609871
[11] X. Li, J.E. Carey, J.W. Sickler, M.U. Pralle, C. Palsule, C.J. Vineis. **20** (5), 5518 (2012). DOI: 10.1364/OE.20.005518
[12] Z. Yan, C. Li, Y. Luo, J. Zhao, H. Yang, P. Verma, S. Kawata. Chin. Opt. Lett., **13** (10), 102401 (2015). DOI: 10.3788/COL201513.102401
[13] X. Qiu, X. Yu, S. Yuan, Y. Gao, X. Liu, Y. Xu, D. Yang. **6**, 1700638 (2018). DOI: 10.1002/adom.201700638
[14] A.C. Ferrari, F. Bonaccorso, V. Falko, K.S. Novoselov, S. Roche, P. Bøggild, S. Borini, F.H. L. Koppens, V. Palermo, N. Pugno, J.A. Garrido, R. Sordano, A. Bianco, L. Ballerini, M. Prato, E. Lidorikis, J. Kivioja, C. Marinelli, T. Ryhänen, A. Morpurgo, J.N. Coleman, V. Nicolosi, L. Colombo, A. Fert, M. Garcia-Hernandez, A. Bachtold, G.F. Schneider, F. Guinea, C. Dekker, M. Barbone, Z. Sun, C. Galiotis, A.N. Grigorenko, G. Konstantatos, A. Kis, M. Katsnelson, L. Vandersypen, A. Loiseau, V. Morandi, D. Neumaier, E. Treossi, V. Pellegrini, M. Polini, A. Tredicucci, G.M. Williams, B.H. Hong, Jong-Hyun, J.M. Kim, H. Zirath, B.J. van Wees, H. van der Zant, L. Occhipinti, A. Di Matteo, I.A. Kinloch, T. Seyller, E. Quesnel, X. Feng, K. Teo, N. Rupesinghe, P. Hakonen, S.R.T. Neil, Q. Tannock, T. Löfwander, J. Kinaret. Nanoscale, **7**, 4598 (2015). DOI: 10.1039/C4NR01600A
[15] A. Pospischil, M. Humer, M.M. Furchi, D. Bachmann, R. Guider, T. Fromherz, T. Mueller. Nature Photon., **7** (11), 892 (2013). DOI: 10.1038/NPHOTON.2013.240
[16] X. Gan, R.-J. Shiue, Y. Gao, I. Meric, T.F. Heinz, K. Shepard, J. Hone, S. Assefa, D. Englund. Nature Photon., **7**, 883 (2013). DOI: 10.1038/nphoton.2013.253
[17] X. Wang, Z. Cheng, K. Xu, H.K. Tsang, J.B. Xu. Nature Photon., **7** (11), 888 (2013). DOI: 10.1038/NPHOTON.2013.241
[18] F. Withers, O. Del Pozo-Zamudio, A. Mishchenko, A.P. Rooney, A. Gholinia, K. Watanabe, T. Taniguchi, S.J. Haigh, A.K. Geim, A.I. Tartakovskii., K.S. Novoselov. Nat Mater., **14** (3), 301 (2015). DOI: 10.1038/nmat4205
[19] M. Liu, X. Yin, E. Ulin-Avila, B. Geng, T. Zentgraf, L. Ju, F. Wang, X. Zhang. Nature, **4474** (7349), 64 (2011). DOI: 10.1038/nature10067
[20] D. Schall, D. Neumaier, M. Mohsin, B. Chmielak, J. Bolten, C. Porschatis, A. Prinzen, C. Matheisen, W. Kuebart, B. Junginger, W. Templ, A.L. Giesecke, H. Kurz. ACS Photon., **1** (9), 781 (2014). DOI: 10.1021/ph5001605
[21] F.H. Koppens, T. Mueller, P. Avouris, A.C. Ferrari, M.S. Vitiello, M. Polini. Nat. Nanotechnol. **9** (10), 780 (2014). DOI: 10.1038/nnano.2014.215
[22] W. Guo, S. Xu, Z. Wu, N. Wang, M.M. T. Loy, S. Du. **9**, 3031 (2013). DOI:10.1002/smll.201370110
[23] Z. Sun, Z. Liu, J. Li, G.-an Tai, S.-P. Lau, F. Yan. Adv. Mater., **24** (43), 5878 (2012), DOI: 10.1002/adma.201202220
[24] G. Konstantatos, M. Badioli, L. Gaudreau, J. Osmond, M. Bernechea, F.P. Garcia de Arquer, F. Gatti, F.H. Koppens. National Nanotechnol., **7** (6), 363 (2012). DOI: 10.1038/nnano.2012.60
[25] M. Freitag, T. Low, W. Zhu, H. Yan, F. Xia, P. Avouris. Nature Commun., **4**, 1951 (2013). DOI: 10.1038/ncomms2951
[26] M. Badioli, A. Woessner, K.J. Tielrooij, S. Nanot, Navickaite, T. Stauber, F.J. Garcıa de Abajo, F.H.L. Koppens. Nano Lett., **14** (11), 6374 (2014). DOI: 10.1021/nl502847v
[27] X. Cai, A.B. Sushkov, R.J. Suess, M.M. Jadidi, G.S. Jenkins, L.O. Nyakiti, R.L. Myers-Ward, S. Li, J. Yan, D.K. Gaskill, T.E. Murphy, H.D. Drew, M.S. Fuhrer. National Nanotechnol., **9**, 814 (2014). DOI: 10.1038/nnano.2014.182
[28] L. Vicarelli, M.S. Vitiello, D. Coquillat, A. Lombardo, A.C. Ferrari, W. Knap, M. Polini, V. Pellegrini, A. Tredicucci. Nature Mater., 11, 865 (2012). DOI: 10.1038/nmat3417
[29] J. Dauber, A.A. Sagade, M. Oellers, K. Watanabe, T. Taniguchi, D. Neumaier, C. Stampfer, Appl. Phys. Lett., 106 (19), (2015). DOI: 10.1063/1.4919897
[30] L. Huang, H. Xu, Z. Zhang, C. Chen, J. Jiang, X. Ma, B. Chen, Z. Li, H. Zhong, L.-M. Peng. Sci. Rep., **4**, 5548 (2014). DOI: 10.1038/srep05548
[31] Q. Wang, W. Hong, L. Dong. Nanoscale, **8**, 7663 (2016). DOI: 10.1039/C5NR09274D
[32] M. Pumera, A. Ambrosi, A. Bonanni, E.L.K. Chng, H.L. Poh. Trends Analyt. Chem., **29** (9), 954 (2010). DOI: 10.1016/j.trac.2010.05.011
[33] A.D. Smith, K. Elgammal, F. Niklaus, A. Delin, A.C. Fischer, S. Vaziri, F. Forsberg, M. Råsander, H. Hugosson, L. Bergqvist, S. Schröder, S. Kataria, M. Östling, M.C. Lemme. Nanoscale, **7**, 19099 (2015). DOI: 10.1039/C5NR06038A
[34] Y. Wu, Y.-m. Lin, A.A. Bol, K.A. Jenkins, F. Xia, D.B. Farmer, Y. Zhu, P. Avouris. Nature, **472**, 74 (2011). DOI: 10.1038/nature09979
[35] B. Radisavljevic, A. Radenovic, J. Brivio, V. Giacometti, A. Kis. National Nanotechnol., **6** (3), 147 (2011). DOI: 10.1038/nnano.2010.279
[36] S. Goossens, G. Navickaite, C. Monasterio, S. Gupta, J.J. Piqueras, R. Pérez, G. Burwell, I. Nikitskiy, T. Lasanta, T. Galán, E. Puma, A. Centeno, A. Pesquera, A. Zurutuza, G. Konstantatos, F. Koppens. Nature Photon., **11**, 366 (2017). DOI: 10.1038/nphoton.2017.75
[37] G. Konstantatos, M. Badioli, L. Gaudreau, J. Osmond, M. Bernechea, F.P. Garcia de Arquer, F. Gatti, F.H. Koppens. National Nanotechnol., **7** (6), 363 (2012). DOI: 10.1038/nnano.2012.60
[38] Z. Sun, Z. Liu, J. Li, G.-A. Tai, S.-P. Lau, F. Yan. Adv. Mater., **24** (43), 5878 (2012). DOI: 10.1002/adma.201202220
[39] A.V. Klekachev, M. Cantoro, M.H. Van Der Veen, A.L. Stesmans, M.M. Heyns, S. De Gendt. Physi. E: Low-Dimensional Systems and Nanostructures, **43** (5), 1046 (2011). DOI: 10.1016/j.physe.2010.12.012
[40] W. Guo, S. Xu, Z. Wu, N. Wang, M.M.T. Loy, S. Du. Small, **9** (18), 3031 (2013). DOI: 10.1002/smll.201370110
[41] S.A. McDonald, G. Konstantatos, S. Zhang, P.W. Cyr., E.J.D. Klem, L. Levina, E.H. Sargent. Nature Mater., **4**, 138 (2005).
[42] V. Barone, O. Hod, G.E. Scuseria. Nano Lett., **6** (12), 2748 (2006). DOI: 10.1021/nl0617033
[43] L. Yang, C.H. Park, Y.W. Son, M.L. Cohen, S.G. Louie. Phys. Rev. Lett., **99** (18), 186801 (2007). DOI: 10.1103/PhysRevLett.99.186801

[44] P.B. Bennett, Z. Pedramrazi, A. Madani, Y.-C.Chen, D.G. de Oteyza, C. Chen, F.R. Fischer, M.F. Crommie, J. Bokor. J. Appl. Phys. Lett., **103** (25), (2013). DOI: 10.1063/1.4855116
[45] J.P. Llinas, A. Fairbrother, G. Borin Barin, W. Shi, K. Lee, S. Wu, B.Y. Choi, R. Braganza, J. Lear, N. Kau, W. Choi, C. Chen, Z. Pedramrazi, T. Dumslaff, A. Narita, X. Feng, K. Müllen, F. Fischer, A. Zettl, P. Ruffieux, E. Yablonovitch, M. Crommie, R. Fasel, J. Bokor. Nature Commun., **8** (1), 633 (2017). DOI: 10.1038/s41467-017-00734-x
[46] B. Jeong, M. Wuttke, Y. Zhou, K. Müllen, A. Narita, K. Asadi. ACS Appl. Electron. Mater., **4**, 2667 (2022). DOI: 10.31613/ceramist.2022.25.4.05
[47] D. Prezzi, D. Varsano, A. Ruini, A. Marini, E. Molinari. Phys. Rev. B, **77**, 041404 (2008). DOI: 10.1103/PhysRevB.77.041404
[48] X. Zhu, H. Su. J. Phys. Chem. A, **115**, 11998 (2011). DOI: 10.1021/jp202787h
[49] P.V. Fedotov, D.V. Rybkovskiy, A.I. Chernov, E.A. Obraztsova, E.D. Obraztsova. J. Phys. Chem. C, **124**, 25984 (2020). DOI: 10.1021/acs.jpcc.0c07369
[50] P.V. Fedotov, E.D. Obraztsova. Appl. Phys. Lett., **122**, 013101 (2023). DOI: 10.1063/5.0131405
[51] P.V. Fedotov, D.V. Rybkovskiy, I.V. Novikov, E.D. Obraztsova. Phys. Status Solidi (b), **259**, 2100501 (2022). DOI: 10.1002/pssb.202100501
[52] J. Cai, P. Ruffieux, R. Jaafar, M. Bieri, T. Braun, S. Blankenburg, M. Muoth, A.P. Seitsonen, M. Saleh, X. Feng, K. Müllen, R. Fasel. Nature, **466**, 470–3 (2010). DOI: 10.1038/nature09211
[53] G. Borin Barin, A. Fairbrother, L. Lukas Rotach, M. Bayle, M. Paillet, L. Liang, V. Meunier, R. Hauert, T. Dumslaff, A. Narita, K. Müllen, H. Sahabudeen, R. Berger, X. Feng, R. Fasel, P. Ruffieux. ACS Appl. Nano Mater., **2**, 2184 (2019). DOI: 10.1021/acsanm.9b00151
[54] H. Huang, D. Wei, J. Sun., S.L. Won, Y. P. Feng, A.C. Neto, A.T.S. Wee, Scientific Reports, **2** (1), 983 (2012). DOI: 10.1038/srep00983
[55] J. Zhou, J. Dong. Appl. Phys. Lett., **91** (17), (2007). DOI: 10.1063/1.2800796
[56] R. Gillen, M. Mohr, C. Thomsen, J. Maultzsch. Phys. Rev. B, **80** (15), 155418 (2009). DOI: 10.1103/PhysRevB.80.155418

Translated by A.Akhtyamov